SCIENTIFIC REPORTS

OPEN

SUBJECT AREAS:
MATERIALS FOR ENERGY AND CATALYSIS
ELECTROCATALYSIS

Received
14 March 2014

Accepted
20 August 2014

Published
10 September 2014

Correspondence and requests for materials should be addressed to P.G. (guopz77@yahoo.com; pzguo@qdu.edu.cn)

Insights into the electrocatalysis of nitrobenzene using chemically-modified carbon nanotube electrodes

Yutao Sang[1], Baoyan Wang[1], Qinchao Wang[1], George Zhao[1,2] & Peizhi Guo[1]

[1]State Key Laboratory Breeding Base of New Fiber Materials and Modern Textile, Collaborative Innovation Centre for Marine Biomass Fibers, Materials and Textiles of Shandong Province, Qingdao University, Qingdao 266071, P. R. China, [2]School of Chemical Engineering, The University of Queensland, St Lucia, QLD 4072, Australia.

The electrochemical behavior of nitrobenzene and its derivatives at chemically-functionalized multi-wall carbon nanotubes (MWNTs) modified electrodes was studied. Experimental results showed that hydroxyl-containing MWNTs exhibited the highest electrocatalytic activity among the used MWNTs because of its weak capacitive features and oxygen-containing functional groups. The cycle voltammetrys of nitrobenzene derivatives on the MWNTs modified electrodes can be easily tuned by changing the substituted groups of nitrobenzene. Based on the experimental data, the electrochemical reaction mechanisms of nitrobenzene and its derivatives on the MWNTs modified electrodes have been discussed and analyzed.

Nitrobenzene (NB) is widely used to produce aniline, dyes, pesticides and drugs in the current industry[1,2]. However, NB is harmful to human health even at low contents[3]. Generally, NB can enter into human body and then lead to serious diseases, such as the attack of nervous and blood system, even liver cancer[4]. Unfortunately, the characteristic of strong electron affinity of the nitro-group in NB makes it stable in the environment. As a result, removal of NB is important, but difficult[5,6].

Recently, the detection and degradation of NB have been developed by using various technologies, such as catalysis and oxidation and reduction processes[7–10]. As a powerful technique, the electrochemical method has been used to detect and degrade NB-rich wastewaters[11–13]. For example, the carbon cloth electrode can be used as the electron donor to selectively degrade NB to aniline in a bioelectrochemical system[11]. Two-dimensional ordered mesoporous carbon nitride was designed as the electrochemical sensor for the detection of NB[12]. The electrochemical degradation of NB has also been comparatively studied in the presence of Fe^{2+}, Cu^{2+} and/or ultraviolet-A light by an oxygen-diffusion cathode[13].

Since the discovery of carbon nanotubes (CNTs)[14], they have been widely used in many important fields, such as energy, catalysis and biomedicine[15–18]. CNTs-based electrodes have been successfully used in the electrocatalysis of various molecules as well as oxygen reduction reaction. For example, multi-wall carbon nanotubes (MWNTs) decorated with Cu/Cu_xO or Pt nanoparticles showed good electrocatalytic activity for NB[19,20]. In the meantime, the electrocatalytic property of CNTs themselves has also been explored[21–24]. For instance, N-doping CNTs showed remarkable electrocatalytic activity toward oxygen reduction reaction[21,22]. It was found that the electrocatalytic activity of MWNTs toward the selective oxidation of dopamine, uric acid and ascorbic acid was closely related to the chemically modified functional groups on MWNTs[23,24]. Despite recent progress, the electrocatalysis of CNTs still needs a further elucidation to gain a better understanding about their intrinsic electrocatalytic ability[20–24].

In this work, MWNTs modified glassy carbon electrodes (MWNTs/GCEs) have been used to investigate the electroreduction of NB in acid electrolytes. The MWNT samples studied in this work included pristine MWNT (MWNT-P), acid-treated MWNT (MWNT-T) and hydroxyl-containing MWNT (MWNT-OH). Based on our previous report[23], MWNT-P contained a small amount of hydroxyl groups, MWNT-T mainly had carboxylic groups with a small part of hydroxyl groups and MWNT-OH contained more hydroxyl groups. It was found that the order of the electrocatalytic activity of the MWNTs/GCEs toward the electroreduction of NB was different from what was observed before[23].

In order to control, detect and degrade NB efficiently and practically, the reduction mechanism of NB on MWNTs/GCEs was investigated systematically by using the cycle voltammetry (CV) technique. Compared with

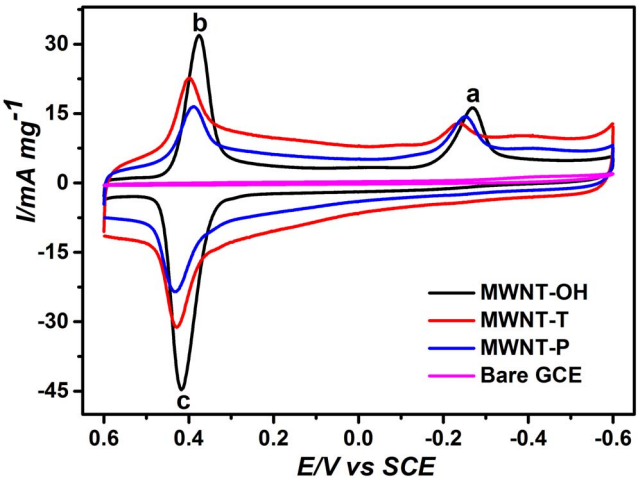

Figure 1 | The performance of MWNT/GCEs for the electrocatalysis of NB. CV curves of different electrodes in aqueous H_2SO_4 (0.2 M) solution containing NB (0.4 mM). All the CV measurements are in the same conditions in this article unless noted otherwise: scan rate: 100 mV/s, sweep interval: 0.001 V, quiet time: 2 sec.

the electroreduction of p-aminophenol, azobenzene and aniline, the results of CV curves revealed an unusual electrochemical reduction pathway for NB and its derivatives on MWNTs/GCEs. NB could be reduced to phenylhydroxylamine, and then generated azobenzene or p-aminophenol by controlling the potential windows.

Results

Figure 1 shows the CV curves of the bare GCE and MWNTs/GCEs measured in aqueous sulphuric acid solutions containing NB. Three peaks can be observed from the CV curves of the MWNTs/GCEs. Peak *a* was produced by the four-electron reduction of NB to phenylhydroxylamine, peaks *b* and *c* were ascribed to the phenylhydroxylamine-nitrosobenzene couple[25]. It can be perceived that the peak current for MWNT-OH/GCE was the highest among the MWNTs/GCEs including the GCE modified with carboxylic-containing MWNT (MWNT-COOH), MWNT-OH with a low –OH content, amino-substituted MWNT (MWNT-NH_2) and graphite (Supplementary Figure S1). Furthermore, the redox peaks of MWNT-OH/GCEs were very sharp. It can be derived that the peak currents of peak *b* were 172, 145 and 302 μA for MWNT-T/GCE, MWNT-P/GCE and MWNT-OH/GCE, respectively. For the MWNT-OH/GCE, redox peaks can also be observed clearly even at a low concentration of NB (Supplementary Figure S2). It is also clear that MWNT-T/GCE showed the highest capacitive feature while MWNT-OH/GCE displayed the lowest capacitive behavior[26].

The differential pulse voltammetry (DPV) curves of MWNT-OH/GCE under varied NB concentrations in aqueous electrolytes were shown in Figure 2A. Clearly, the peaks currents continued to rise with the increase of NB concentration. It can be concluded that DPV curves of the electrode showed a higher sensitivity than CV curves (Supplementary Figure S3). The inset in Figure 2A revealed that MWNT-OH/GCE presented a linear relationship within the studied concentrations of NB, with a correlation coefficient of $r = 0.999$. The detection limit of NB on MWNT-OH/GCE was calculated to be about 0.08 μM. However, the detection limits of NB were 1.5 and 2.5 μM for MWNT-P/GCE and MWNT-T/GCE, respectively (see Supplementary Figure S4).

Figure 2B shows the CV curves of MWNT-OH/GCE in 0.2 M H_2SO_4 electrolytes with 0.4 mM NB at various scan rates. The symmetrical and good redox peaks of NB on MWNT-OH/GCE can be observed. The potentials of oxidation peak *3* and reduction peak *2* were 367.6 and 348.8 mV at the scan rate of 20 mV/s, respectively, indicating that the electrochemical reactions for the electrocatalysis of NB were reversible at the electrode. With the scan rate up to 160 mV/s, the peak separation (ΔEp) of peaks *2* and *3* was slightly increased to 44.4 mV. The inset in Figure 2B showed that all the peak currents increased linearly with the square root of the scan rates, suggesting the existence of a surface diffused process[27].

Discussion

The above results indicated that MWNT-OH/GCE exhibited an excellent electrocatalytic activity for NB and this is the consequence of the interactions among several factors. In our previous report[23], however, MWNT-T/GCEs showed the highest activity toward simultaneously detecting dopamine, uric acid and ascorbic acid in aqueous electrolytes. It had been revealed that the order of oxygen-containing functional groups in CNTs was MWNT-T > MWNT-COOH > MWNT-OH > MWNT-P, and most of the functional groups in MWNT-T were carboxyl groups[23]. Therefore, the lack of sufficient groups in MWNT-P as well as graphite (Supplementary Figure S1) turned out to be the worst electrocatalytic performance for both NB and the mixed systems[23]. As depicted in Figure 1, however, more functional groups in MWNT-T increase the capacitive behavior compared with those of MWNT-OH and MWNT-P, which may hinder the electrocatalytic activity of MWNT-T, especially for the detection of NB. It is generally known that the wall of MWNTs is built up by the π electron delocalization from sp^2 hybrid orbitals, thus it's readily for MWNTs to interact with other substances which contain π electrons and this should not cause any destruction to the structure of the chemically-modified MWNTs. The hydroxyl or amino group on the surface or the edge of the MWNTs is a strong electron donor, which would increase the electron density and strengthen the electron delocalization of MWNTs. However, most of the functional groups in MWNT-T are carboxyl groups and the carboxyl group is a kind of strong electron acceptors[23]. In the meanwhile, the reduction of NB is a process of received electrons. Therefore, the more electron donors modified in MWNTs, the higher electron density of MWNTs and the more readily reduction of NB (Figure S1). The order of hydroxyl-containing functional groups in CNTs was MWNT-OH > MWNT-T > MWNT-P which is consistent with the order of electrocatalytic activity as depicted in Figure 1. Clearly, the increase of the content of hydroxyl or amino groups in MWNTs could enhance their electrocatalytic activity toward the electroreduction of NB (Figure S1). It was also proposed that the specific surface areas of MWNTs should contribute to the electrocatalytic performances of chemically-modified MWNTs, which were >233 m^2/g, 40–300 m^2/g, and >40 m^2/g for MWNT-NH_2, MWNT-OH and MWNT-OH with less hydroxyl groups, respectively, according to the product descriptions.

To calculate the removal efficiency of NB, DPV measurements of NB on the modified GCEs were performed. Supplementary Figure S5 shows the DPV curves of NB on MWNT-OH/GCE at different scanning cycles. The peak current reached a maximum (1.07 mA) within 10 scan cycles and then decreased slowly along with the continuous measurements. First cycle was chosen as the baseline because of no peak at the potential of 0.35 V. According to the Faraday's law of electrolysis, the removal rate of NB is estimated to be 0.41, 0.28 and 0.33 mg for MWNT-OH, MWNT-P and MWNT-T per mg after 200 scanning cycles. At the same time, MWNT-OH/GCE still maintained a high electrocatalytic activity for NB with the performance only decreased 32% after repeated used for 200 times (Supplementary Figure S5). Therefore, MWNT-OH was selected to investigate the electrocatalytic mechanism of NB.

When the potential window was extended, an interesting change in the CV curves of MWNT-OH/GCE can be observed (Figure 3A). When the positive potential is less than 0.30 V, only peak *a* can be obtained. With the positive potential increased to 0.50 V, the observed green curve in Figure 3A is similar to those in Figure 2B.

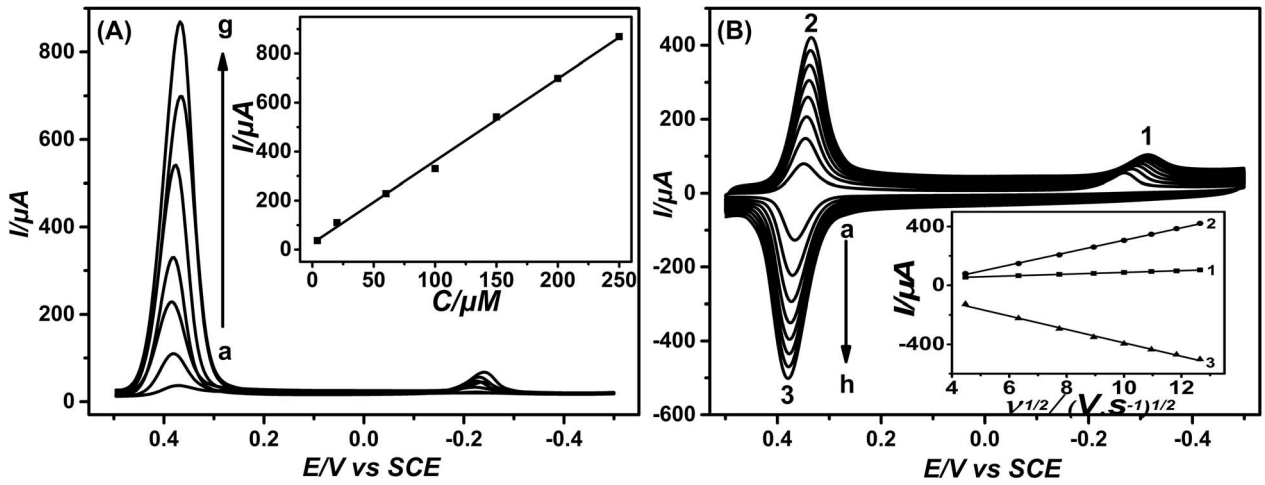

Figure 2 | The influence of concentrations and scan rates for MWNT-OH. (A) DPV curves of NB under different concentrations: (a) 4, (b) 20, (c) 60, (d) 100, (e) 150, (f) 200, (g) 250 μM. DPV conditions: scan rate: 20 m/s, amplitude: 50 mV, pulse width: 50 ms, pulse period: 200 ms; (B) CV curves of NB (0.4 mM) on MWNT-OH/GCE in aqueous H_2SO_4 (0.2 M) solution at various scan rates: (a) 20, (b) 40, (c) 60, (d) 80, (e) 100, (f) 120, (g) 140, (h) 160 mV/s. Inset shows variations of current vs. the square root of scan rate.

However, the pink curve was different from that in Figure 1 when the ending potential was 0.60 V. This is because the pink curve was obtained after several circular scans in order to appear peaks *g* and *h*. Similar redox peaks can also be observed for the blue curves with the positive potential slightly increased, indicating that peaks *g* and *h* were a pair of redox peaks. Besides, peaks *c* and *d* were little lower than these used to be, probably ascribed to the formation of peaks *g* and *h*. Further increasing the potential led to the appearance of three pairs of redox couple peaks, namely peaks *c* and *d*, *g* and *h*, *e* and *f*. It was seen that peaks *b* and *i* appeared with the ΔEp of 678.7 mV when the sweeping range was set from −0.50 ~ 1.0 V. In the meantime, the ΔEp values of other three couples were very small, indicating the existence of the reversible response for these redox peaks. Obviously, both MWNT-P and MWNT-T showed less electrocatalytic performances than MWNT-OH (Supplementary Figure S6).

In order to see the change of these redox peaks clearly, the CV curves were conducted continuously more than 100 circles, as shown in Figure 3B. It can be seen that there was no peak in the first scanning segment from 0 V to 1.0 V. In the second segment, NB began to be reduced at −0.302 V (peak *a*), and then a new oxidation peak *d* was obtained at 0.370 V in the return cycle. Another new reduction peak *c* was observed at 0.342 V in the next segment. This indicated that peaks *c* and *d* were generated by the intermediate which was formed during the reduction process of NB. With the increase of the scan segments, peaks *b* and *i* appeared almost at the same time, and then a pair of reversible redox peaks (peaks *e* and *f*) were observed at ~0.475 V. At last, another pair of reversible redox peaks (peaks *g* and *h*) was obtained at ~0.575 V. In short, the peaks in the wide potential range during the electroreduction of NB at MWNT-OH/GCE followed the pathway: peak *a* → pecks *c* and *d* → peaks *b* and *i* → peaks *e* and *f* → peaks *g* and *h*.

However, the electroreduction of NB derivatives on MWNT-OH/GCE was rather different from that of NB (Figures 3C, D and Supplementary Figure S7). As depicted in Figure 3C, adding a methyl group in the para position of NB (namely p-nitrotoluene) led to the disappearance of one pair of redox peaks at the potential of about 0.60 V in the scanning window of 0.50 ~ −1.0 V compared with that of NB. However, the CV curves for the electroreduction of p-nitrophenol only showed one pair of redox peaks at about 0.50 V under the largest potential window due to the existence of a hydroxyl group in the molecule (Figure 3D). It is also found that the CV curves for the electrocatalysis of both m-dinitrobenzen and 2,4-dinitrotoluene displayed one couple of peaks at about 0.38 V and two peaks at the potential range of 0.10 V ~ 0.30 V with positive electrocatalytic currents (Supplementary Figure S7). These indicated that the electrocatalytic reactions of aromatic nitro compounds on the CNT-GCEs can be easily adjusted by changing the substituted groups in the molecule.

The electrochemical reduction of NB may produce a variety of intermediates, including phenylhydroxylamine, aniline, azoxybenzene and azobenzene, etc[2,25]. It is proposed that peaks *e*, *f*, *g* and *h* should be related to the reduction of aniline. To demonstrate this hypothesis, CV measurements of aniline on MWNT-OH/GCE were performed (Figure 4A). For aniline, an oxidation peak *i′* at 0.87 V was observed in the first scanning segment, and two reduction peaks could be obtained at 0.58 V (peak *g′*) and 0.47 V (peak *e′*) in the return segment, and then another two oxidation peaks *f′* and *h′* were observed subsequently almost at the same potentials for peaks *e′* and *g′*, respectively. With the increase of scanning laps, the catalytic current of peak *i′* diminishs, but the other two pairs of reversible peaks rose. These indicated that these two pairs of reversible peaks were attributed to the reduction of peak *i′*.

When the potential window was narrowed at 0.8 V, another pair of redox peak (peaks *j′* and *k′*) was observed at 0.4 V (Supplementary Figure S8). In the meantime, the former two pairs of peaks sharply reduced, indicating that the scanning potential has a great effect on the behavior of aniline on the MWNTs modified electrodes. It is reported that these pairs of redox peaks were generated during the degradation of polyaniline[28–30]. Peaks *e′* and *f′* were ascribed to the p-aminophenol and p-benzoquinoneimine couple, while peaks *j′* and *k′* were attributed to the benzoquinone and hydroquinone couple[31–33]. These observations can also been proved by the CV curves of aniline, hydroquinone, p-aminophenol (Supplementary Figure S9) on the MWNT-OH/GCE.

To prove the above deduction and deeply explain the electrochemical reduction of NB, the CV curves of NB, p-aminophenol, azobenzene and aniline were overlapped under a similar experimental condition (Figure 4B). Clearly, the potentials of redox peaks for p-aminophenol and azobenzene are equal to the peaks *e* and *f*, peaks *g* and *h* of NB respectively, indicating that peaks *e* and *f* put down to the p-aminophenol and p-benzoquinoneimine couple and peaks *g* and *h* attribute to azobenzene and hydrazobenzene couple. So, it is suggested that the evolution of NB on the MWNT-GCEs should be undergone the electroreductive pathway as described as Figure 5. Peak *a* was first generated by the four-electron reduction of NB to phenylhydroxylamine, then phenylhydroxylamine continued to be

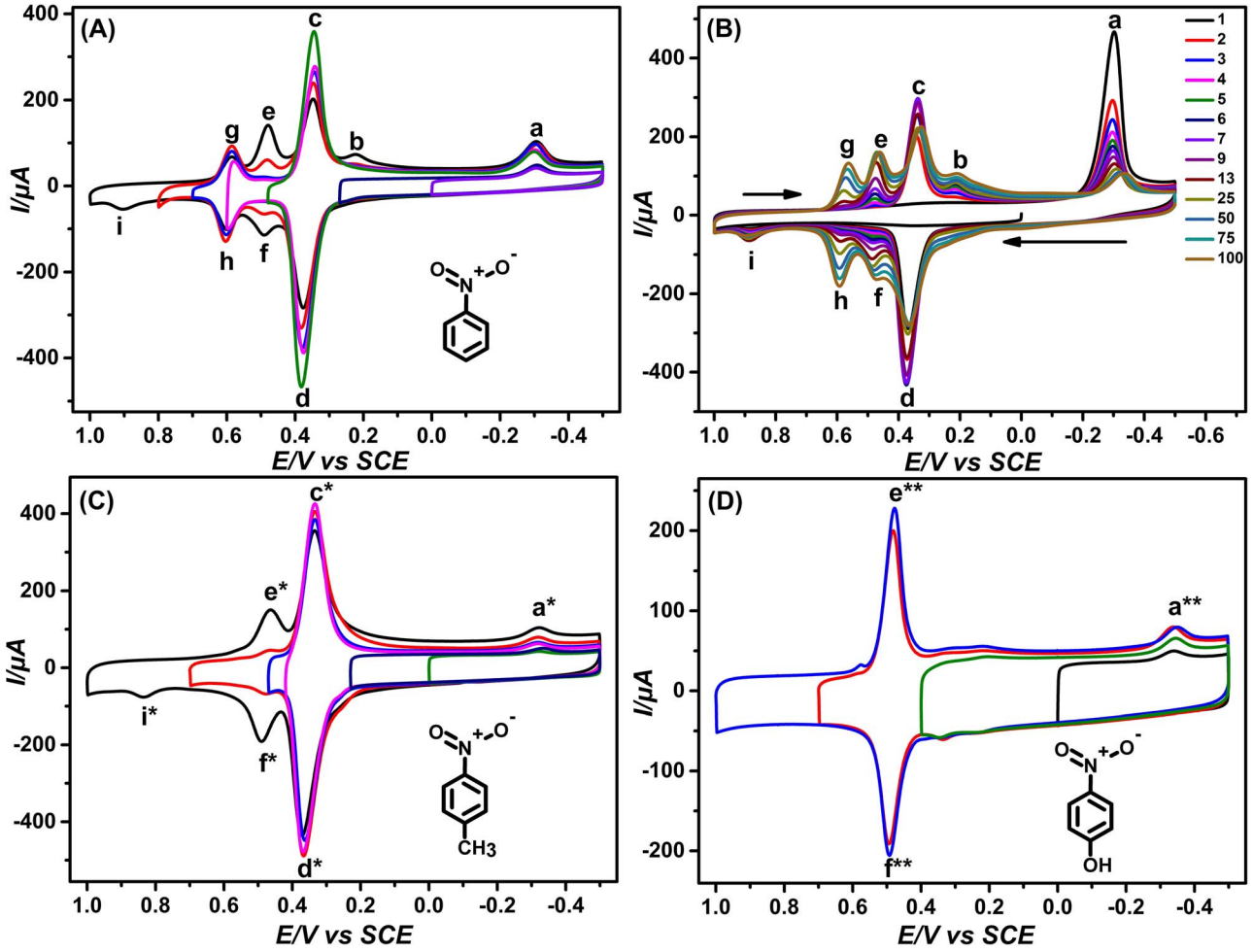

Figure 3 | The influence of varied potential windows (A, C & D) and circular sweeps (B) for MWNT-OH. CV curves of (A & B): NB (0.4 mM), (C): p-nitrotoluene (0.4 mM), (D): p-nitrophenol (0.4 mM) in H_2SO_4 (0.2 M) solutions. For (B), CV curves began at the potential of 0 V and shifted to positive potential, it didn't shift back until reached 1 V, then went back at the potential of −0.5 V. Thus, the curves went back and forth between 1 V and −0.5 V. The arrow indicates scan direction.

oxidized to nitrosobenzene (peaks *c* and *d*). With the increase of the scan segments, it is proposed that two separated reductive pathways can be generated by phenylhydroxylamine. On the one hand, p-aminophenol can be formed by the Bamberger rearrangement from phenylhydroxylamine and then p-aminophenol was oxidized to p-benzoquinoneimine (peaks *e* and *f*)[34]. On the other hand, azobenzene

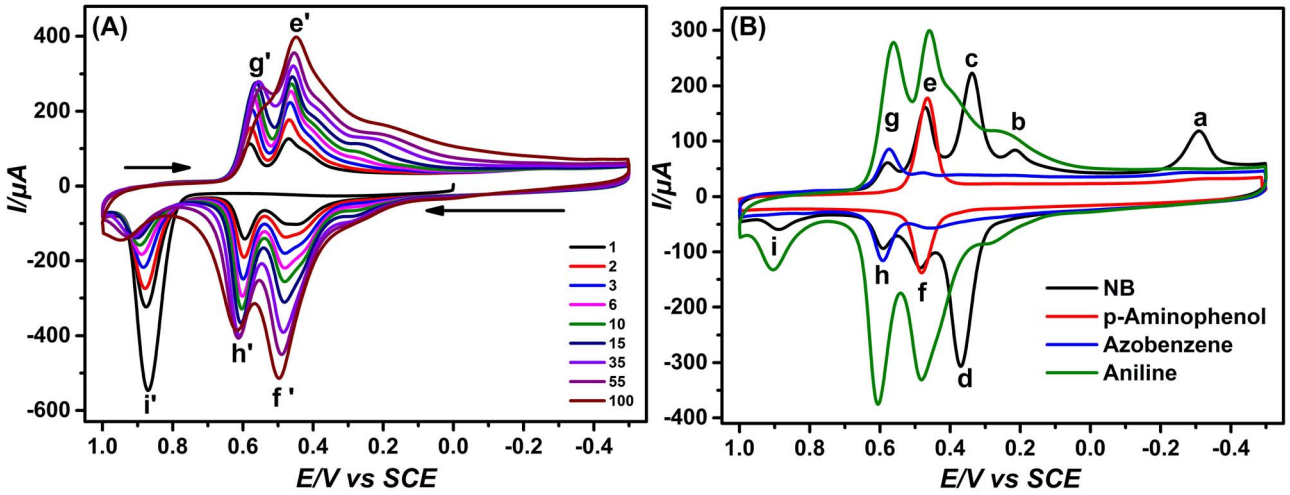

Figure 4 | The performance of aniline, p-aminophenol and azobenzene on MWNT-OH/GCE. (A) CV curves of aniline (0.5 mM) with varied scan cycles, (B) CV curves of NB (0.4 mM), aniline (0.5 mM), p-aminophenol (0.4 mM) and azobenzene (0.4 mM). Each of them is dissolved in the H_2SO_4 (0.2 M) solution. The arrows in Figure 4A indicate the scan direction.

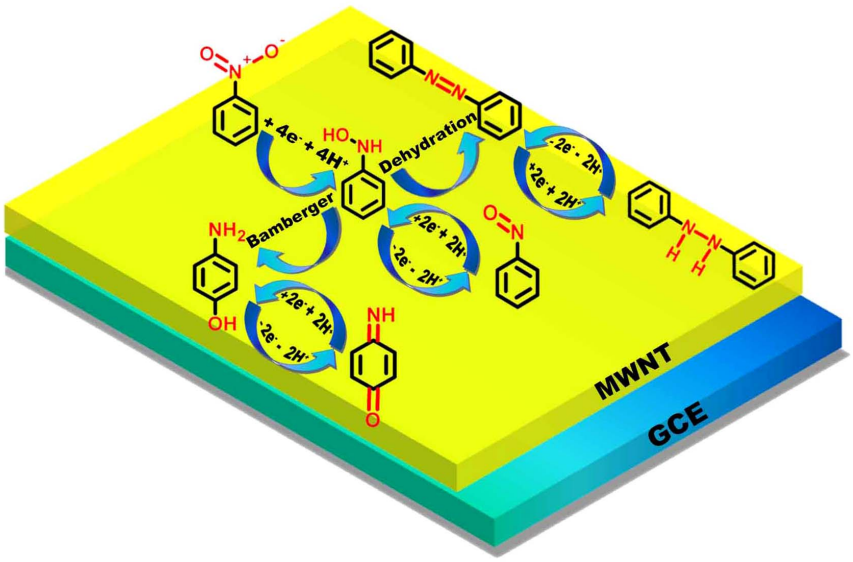

Figure 5 | **The possible electroreductive mechanism of NB on the MWNTs/GCEs.**

may be produced from phenylhydroxylamine by dehydration synthesis and azobenzene can be reduced to hydrazobenzene by getting two-electron (peaks *g* and *h*). However, p-aminophenol would not be generated if the potential was lower than 0.80 V. It is also suggested that the as-formed azobenzene and hydrazobenzene can be interacted with MWNTs through the π-π interactions due to their conjugated systems[35]. The combined effects of these interactions among the intermediate compounds and MWNTs would lead to the specificity of the products and the subsequently electrochemical reaction will become more complicated as the reaction time increases, resulting in the formation of more complicated compounds.

It is proposed that the existence of the methyl group in p-nitrotoluene should influence the further reaction of 4-(hydroxyamino)toluene (Figure 6A), which was first formed by the electroreduction of p-nitrotoluene. Thus, 4-(hydroxyamino)toluene was transformed to 2-amino-5-methylphenol later via the Bamberger rearrangement[34]. The CV curves of p-nitrophenol and p-aminophenol are almost completely overlapped except the peak *a*, indicating that the p-aminophenol and p-benzoquinoneimine are the ended products of the reduction of p-nitrophenol (Supplementary Figure S10). Peak *a* appears at the same potential (−0.34 V) with that of NB and it's ascribed to the four-electron reduction from the nitro to hydroxyamino group[25]. Because of the conjugated system between the phenyl and hydroxyl group, 4-(hydroxyamino)phenol generates p-aminophenol by getting two-electron directly without oxidized to p-benzoquinoneimine similar to those results about NB. Therefore, peaks *c* and *d* are not observed from the CV curves of p-nitrophenol (Figure 3D).

To conclude, the electroreduction of NB on MWNTs/GCEs was found to be dependent on the surface functional groups of MWNTs, in which the hydroxyl group plays a key role during the electroreduction process. So MWNT-OH exhibited a higher catalytic activity than MWNT-T although MWNT-T has more functional groups. The capacitive feature of MWNT-T might impede the sensitivity for the electroreduction of NB on MWNTs/GCEs. It is suggested that NB should first generate phenylhydroxylamine by the four-electron reduction, and then phenylhydroxylamine can be oxidized to nitrosobenzene by losing two electrons. Phenylhydroxylamine can be transformed to azobenzene by losing two water molecules and azobenzene was reduced to hydrazobenzene after getting two hydrogen atoms. If the scanning potential was over 0.80 V, phenylhydroxylamine would generate p-aminophenol through the Bamberger rearrangement, which was then oxidized to p-benzoquinoneimine by losing two electrons. The redox reactions between phenylhydroxylamine and nitrosobenzene, azobenzene and hydrazobenzene, p-aminophenol and p-benzoquinoneimine show visible reversibility according to the CV measurements. Because of the existence of the methyl or hydroxyl group, the electroreductive mechanism of

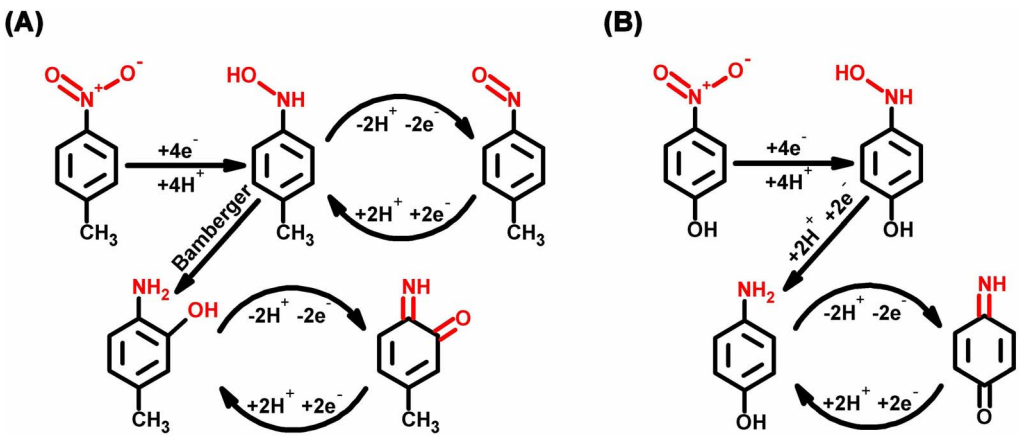

Figure 6 | **The possible electroreductive mechanisms of (A) p-nitrotoluene and (B) p-nitrophenol on electrode MWNT-OH/GCE.**

p-nitrotoluene and p-nitrophenol on MWNTs/GCEs was slightly different from that of NB. These should help the design of newly electrochemical sensors based on CNTs.

Methods

Preparation of the modified electrodes. The bare GCE was polished to a mirrorlike surface with 0. 3 μm Al_2O_3 and rinsed with deionized water, then ultrasonicated in ethanol and deionized water for 15 minutes. Finally, the bare electrode was washed with deionized water and dried under ambient conditions. MWNTs (1 mg) were dispersed into 1 mL 0.05% nafion solution by ultrasonication to obtain a well-dispersed suspension. 10 μL of the suspension was dispensed on the treated bare GCE and exposed to air for 30 min at room temperature before electrochemical measurements.

Electrochemical measurements. The electrochemical experiment was performed on a three-electrode system with MWNTs/GCEs as the working electrode, a platinum foil as the counter electrode and a saturated calomel electrode as the reference electrode. The modified electrode was scanned in H_2SO_4 solutions (0.2 M), and then in the same solution containing NB with desired concentrations. CV and DPV were measured in a CHI 760E electrochemical workstation (CH Instruments, USA). All measurements were done at room temperature.

1. Sarasa, J. *et al*. Treatment of a wastewater resulting from dyes manufacturing with ozone and chemical coagulation. *Water Res.* **32**, 2721–2727 (1998).
2. Agrawal, A. & Tratnyek, P. G. Reduction of nitro aromatic compounds by zero-valent iron metal. *Environ. Sci. Technol.* **30**, 153–160 (1996).
3. Hrapovic, S., Majid, E., Liu, Y., Male, K. & Luong, J. H. T. Metallic nanoparticle-carbon nanotube composites for electrochemical determination of explosive nitroaromatic compounds. *Anal. Chem.* **78**, 5504–5512 (2006).
4. Holder, J. W. Nitrobenzene potential human cancer risk based on animal studies. *Toxicol. Ind. Health.* **15**, 458–463 (1999).
5. Van der Zee, F. P., Lettinga, G. & Field, J. A. Azo dye decolourisation by an anaerobic granular sludge. *Chemosphere* **44**, 1169–1176 (2001).
6. Nielsen, P. H. & Christensen, T. H. Variability of Biological Degradation of Phenolic Hydrocarbons in an Aerobic Aquifer Determined by Laboratory Batch Experiments. *J. Contam. Hydrol.* **17**, 55–67 (1994).
7. Tanaka, A. *et al*. Functionalization of a plasmonic Au/TiO_2 photocatalyst with an Ag co-catalyst for quantitative reduction of nitrobenzene to aniline in 2-propanol suspensions under irradiation of visible light. *Chem. Commun.* **49**, 2551–2553 (2013).
8. Gao, Y. J., Ma, D., Wang, C. L., Guan, J. & Bao, X. H. Reduced graphene oxide as a catalyst for hydrogenation of nitrobenzene at room temperature. *Chem. Commun.* **47**, 2432–2434 (2011).
9. Zhu, H. Y., Ke, X. B., Yang, X. Z., Sarina, S. & Liu, H. W. Reduction of nitroaromatic compounds on supported gold nanoparticles by visible and ultraviolet Light. *Angew. Chem. Int. Ed.* **49**, 9657–9661 (2010).
10. Corma, A., Concepción, P. & Serna, P. A different reaction pathway for the reduction of aromatic nitro compounds on gold catalysts. *Angew. Chem. Int. Ed.* **46**, 7266–7269 (2007).
11. Wang, A. J. *et al*. Efficient reduction of nitrobenzene to aniline with abiocatalyzed cathode. *Environ. Sci. Technol.* **45**, 10186–10193 (2011).
12. Zhang, Y. F. *et al*. Fabrication of 2D ordered mesoporous carbon nitride and its use as electrochemical sensing platform for H_2O_2, nitrobenzene, and NADH detection. *Biosens. Bioelectron.* **53**, 250–256 (2013).
13. Brillas, E. *et al*. Catalytic effect of Fe^{2+}, Cu^{2+} and UVA light on the electrochemical degradation of nitrobenzene using an oxygen-diffusion cathode. *New. J. Chem.* **28**, 314–322 (2004).
14. Iijima, S. Single-shell carbon nanotubes of 1-nm diameter. *Nature* **354**, 56–58 (1991).
15. Hao, F. *et al*. High Electrocatalytic Activity of Vertically Aligned Single-Walled Carbon Nanotubes towards Sulfide Redox Shuttles. *Sci. Rep.* **2**, 368 (2012).
16. Zebda, A. *et al*. Mediatorless high-power glucose biofuel cells based on compressed carbon nanotube-enzyme electrodes. *Nat. Commun.* **2**, 370 (2011).
17. Chen, T., Peng, H. S., Durstock, M. & Dai, L. M. High-performance transparent and stretchable all-solid supercapacitors based on highly aligned carbon nanotube sheets. *Sci. Rep.* **4**, 3612 (2014).
18. Cai, L. *et al*. Super-stretchable, Transparent Carbon Nanotube-Based Capacitive Strain Sensors for Human Motion Detection. *Sci. Rep.* **3**, 3048 (2013).
19. Sheng, X. *et al*. Cu/Cu_xO and Pt nanoparticles supported on multi-walled carbon nanotubes as electrocatalysts for the reduction of nitrobenzene. *Appl. Catal. B* **147**, 330–339 (2014).
20. Sun, Z. Y. *et al*. The solvent-free selective hydrogenation of nitrobenzene to aniline: an unexpected catalytic activity of ultrafine Pt nanoparticles deposited on carbon nanotubes. *Green Chem.* **12**, 1007–1011 (2010).
21. Gong, K., Du, F., Xia, Z., Durstock, M. & Dai, L. Nitrogen-doped carbon nanotube arrays with high electrocatalytic activity for oxygen reduction. *Science* **323**, 760–764 (2009).
22. Zhao, Y. *et al*. Can boron and nitrogen co-doping improve oxygen reduction reaction activity of carbon nanotubes? *J. Am. Chem. Soc.* **135**, 1201–1204 (2013).
23. Bi, H. Q. *et al*. Carbon-nanotube-modified glassy carbon electrode for simultaneous determination of dopamine, ascorbic acid and uric acid: The effect of functional groups. *Sensors Actuat. B: Chem.* **171**, 1132–1140 (2012).
24. Habibi, B. & Pournaghi-Azar, M. H. Simultaneous determination of ascorbic acid, dopamine and uric acid by use of a MWCNT modified carbon-ceramic electrode and differential pulse voltammetry. *Electrochim. Acta.* **55**, 5492–5498 (2010).
25. Li, Y. U., Cao, H. B., Liu, C. M. & Zhang, Y. Electrochemical reduction of nitrobenzene at carbon nanotube electrode. *J. Hazard. Mater.* **148**, 158–163 (2007).
26. Lu, W., Hartman, R., Qu, L. T. & Dai, L. M. Nanocomposite Electrodes for High-Performance Supercapacitors. *J. Phys. Chem. Lett.* **2**, 655–660 (2011).
27. Laviron, E., Roullier, L. & Degrand, C. A multilayer model for the study of space distributed redox modified electrodes. 2. Theory and application of linear potential sweep voltammetry for a simple reaction. *J. Electroanal. Chem.* **112**, 11–23 (1980).
28. Dinh, H. N., Ding, J., Xia, S. J. & Birss, V. I. Multi-technique study of the anodic degradation of polyaniline films. *J. Electroanal. Chem.* **459**, 45–56 (1998).
29. Zhang, A. Q., Cui, C. Q. & Lee, J. M. Electrochemical degradation of polyaniline in $HClO_4$ and H_2SO_4. *Synthetic. Met.* **72**, 217–223 (1995).
30. Arsov, L. D., Plieth, W. & Koûmehl, G. Electrochemical and Raman spectroscopic study of polyaniline; influence of the potential on the degradation of polyaniline. *J. Solid State Electrochem.* **2**, 355–361 (1998).
31. Stilwell, D. E. & Park, S. M. Electrochemistry of conductive polymers. V: In situ spectroelectrochemical studies of polyaniline. *J. Electrochem Soc.* **135**, 2254–2261 (1988).
32. Wang, Z. H., Li, X., Wu, Y., Tang, Y. H. & Ma, S. H. Spectroelectrochemistry for a coupled chemical reaction in the channel cell: Part II. Kinetics of hydrolysis and the absorption spectrum of p-benzoquinoneimine. *J. Electroanal. Chem.* **464**, 181–186 (1999).
33. Kobayashi, T., Yoneyama, H. & Tamura, H. Polyaniline film-coated electrodes as electrochromic display devices. *J. Electroanal. Chem.* **161**, 419–423 (1984).
34. Bamberger, E. Über das phenylhydroxylamin. I. Mittheilung über alkylhydroxylamine. *Chem. Ber.* **27**, 1347–1350 (1894).
35. Hunter, C. A. & Sanders, J. K. M. The nature of π-π interactions. *J. Am. Chem. Soc.* **112**, 5525–5534 (1990).

Acknowledgments

This work was financially supported by the National Natural Science Foundation of China (No. 21143006 and U1232104).

Author contributions

Y.S., B.W. and P.G. conceived and designed the experiments. Y.S., B.W. and Q.W. performed the experiments. Y.S., G.Z. and P.G. analysed the data and wrote the paper. All authors discussed and commented on the manuscript.

Additional information

Supplementary information accompanies this paper at http://www.nature.com/scientificreports

Competing financial interests: The authors declare no competing financial interests.

How to cite this article: Sang, Y., Wang, B., Wang, Q., Zhao, G. & Guo, P. Insights into the electrocatalysis of nitrobenzene using chemically-modified carbon nanotube electrodes. *Sci. Rep.* **4**, 6321; DOI:10.1038/srep06321 (2014).